



Proceedings
Conference on Structures for
Mining and Related Materials Handling
2012

Riverside Lifestyle Resort, Vanderbijlpark, South Africa
15-18 October 2012

Organised by the
Southern African Institute of Steel Construction



SMMH2012 PROCEEDINGS SPONSOR



Proceedings of the Structures for Mining and Related Materials Handling Conference 2012

The opinions, findings, conclusions and recommendations expressed in this publication are those of the authors and do not necessarily reflect the views of the organisers or sponsors of the SMMH2012 Conference.

Compiled and published by

SA Institute of Steel Construction
43 Empire Road
Johannesburg
South Africa
Telephone: +27 (0)11 726 6111
Fax: +27 (0)11 482 9644
Web: www.saisc.co.za

Printed by Minuteman Press, Alberton, South Africa

ISBN: 978-0-620-54829-8

October 2012

Copyright © Southern African Institute of Steel Construction

Extracts of this publication may be reproduced provided that prior permission is obtained from the publisher and full acknowledgement is given.

The text of the papers in this publication was set individually.

6.5.1 CONNECTION DESIGN FOR INDUSTRIAL STRUCTURES — PROBLEMS AND SOLUTIONS

Dr Bo Dowswell, ARC International, LLC

This paper presents solutions to three common problems encountered in connection design for industrial structures: 1. Design of wrap-around gusset plates, 2. Uplift at base chair connections, 3. Fatigue of coped beams.

1 WRAP-AROUND GUSSET PLATES

Where a horizontal brace is located at a beam-to-column intersection, the gusset plate must be cut out around the column as shown in Figure 1. Due to the unconventional geometry, flexural stresses develop in the plate that must be accounted for in design. A design procedure for these “wrap-around” gusset plates is presented here, which is based on experimental testing and finite element models by the author.

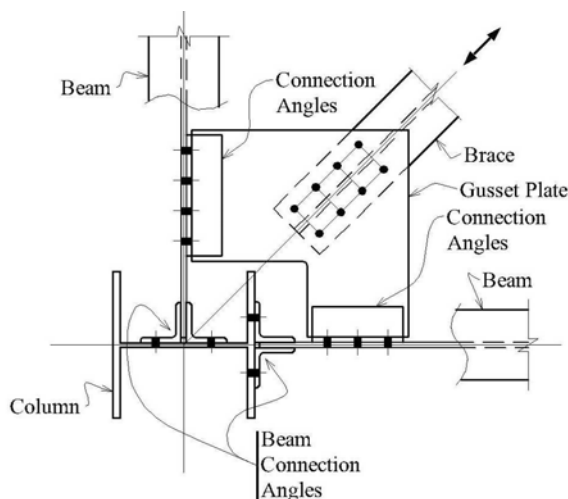


Figure 1: Horizontal brace connection at beam-to-column intersection.

1.1 Load Distribution

The assumed load distribution in wrap-around gusset plate connections is shown in Figure 2. Each leg of the plate is subject to limit states common to flexural members; therefore, each leg is modeled independently as a cantilever beam. In addition to the flexural strength, which will be discussed in this paper, the shear strength of each leg should be considered in the design.

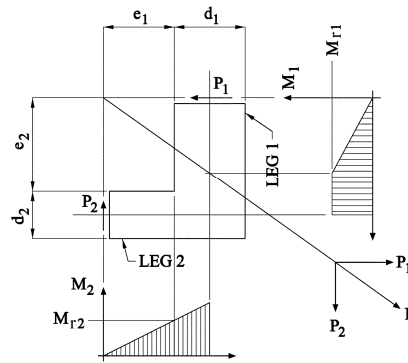


Figure 2: Force system for wrap-around gusset plates.

Each leg of the gusset plate must resist the flexural stresses generated by the load system in Figure 2. This load system results in maximum bending moments at the reentrant corner where the two legs meet. The required bending moments at the critical sections of the plate are

$$M_{r1} = P_1 e_2 \quad (1a)$$

$$M_{r2} = P_2 e_1 \quad (1b)$$

where

P_1, P_2 = components of the brace load, P (see Figure 2)

e_1, e_2 = cutout dimensions at each leg (see Figure 2)

1.2 Strength of Gusset Plate Legs

Tests and finite element models (Dowswell, 2005) showed that the flexural stresses in the legs can cause buckling, even if the brace is loaded in tension. All of the test specimens had a permanent out-of-plane deformation at the plate edges with flexural compression stresses. The out-of-plane deformation was accompanied by twisting of the gusset plate legs, indicating a lateral-torsional buckling failure. The typical buckled shapes of the finite element models are shown in Figures 3a and 3b for tension and compression brace loads respectively.

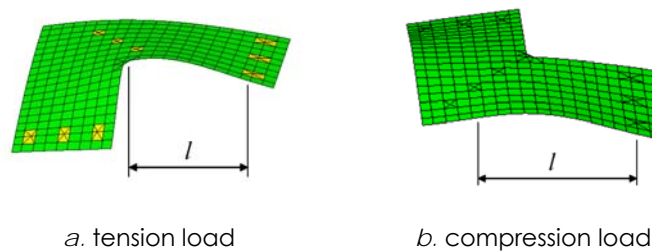


Figure 3. Buckled shapes.

For the design to be adequate using LRFD design, Equations 2a and 2b must be satisfied

$$\phi M_{n1} \geq M_{r1} \quad (2a)$$

$$\phi M_{n2} \geq M_{r2} \quad (2b)$$

where

$$\phi = 0.90$$

AISC *Specification* (AISC, 2010) Section F11 defines the flexural strength of rectangular members. The nominal strength is the lower value obtained according to the limit states of yielding and lateral-torsional buckling.

For $\frac{L_b d}{t^2} \leq \frac{0.08E}{F_y}$, yielding is the controlling limit state. The nominal strength is

$$M_n = M_p = F_y Z \leq 1.6M_y \quad (3)$$

For $\frac{0.08E}{F_y} < \frac{L_b d}{t^2} \leq \frac{1.9E}{F_y}$, inelastic lateral-torsional buckling is the controlling limit state.

$$M_n = C_b \left[1.52 - 0.274 \left(\frac{L_b d}{t^2} \right) \frac{F_y}{E} \right] M_y \leq M_p \quad (4)$$

For $\frac{L_b d}{t^2} > \frac{1.9E}{F_y}$, elastic lateral-torsional buckling is the controlling limit state.

$$M_n = F_{cr} S_x \leq M_p \quad (5)$$

where

$$F_{cr} = \frac{1.9EC_b}{\frac{L_b d}{t^2}}$$

C_b = modification factor for nonuniform moment diagrams

E = modulus of elasticity, MPa

F_y = specified minimum yield strength, MPa

L_b = distance between brace points, mm

M_p = plastic moment capacity, N-mm

M_y = elastic yield moment, N-mm

S_x = elastic section modulus, mm³

Z = plastic section modulus, mm³

d = depth of gusset leg, mm

t = thickness of gusset plate, mm

Using equations developed by Dowswell (2004) for wide flange cantilever beams, $C_b = 1.84$ is appropriate for beams braced at both ends. However, the experimental and finite element results show that the legs can be assumed fully braced at both ends only under certain conditions. Geometry dictates that, in most cases, both legs will not reach their critical load simultaneously. Therefore, the non-critical (adjacent) leg can provide restraint to the critical leg and $C_b = 1.84$ is accurate. Conversely, when the critical load ratio of both legs are similar, full bracing cannot be assumed, and $C_b = 1.00$ is more accurate. The modification factor, C_b , can be determined based on the critical load ratio, α .

$$\alpha = \frac{(M_{cr}/M_r)_A}{(M_{cr}/M_r)_C} \quad (6)$$

where

$(M_{cr}/M_r)_A$ = ratio of critical moment to required moment at the adjacent leg

$(M_{cr}/M_r)_C$ = ratio of critical moment to required moment at the critical leg

$M_{cr} = F_{cr}S_x$

For gusset plates carrying tensile brace loads, $C_b = 1.84$

For gusset plates carrying compressive brace loads with $\alpha \geq 1.5$, $C_b = 1.84$

For gusset plates carrying compressive brace loads with $\alpha < 1.5$, $C_b = 1.00$

To determine the buckling length, L_b , the buckled shape of the specimens and finite element models was observed. For the specimens loaded in tension, the inside edges buckled farther than the outside edges as shown in Figure 3a. This behavior was expected because the maximum compressive flexural stresses are on the inside edges at the reentrant corner. The specimens loaded in compression buckled farther on the outside edges as shown in Figure 3b. The buckling length of the tension specimens was limited to the cutout dimension; however, the buckling length for the compression specimens extended much farther beyond the cutout.

The following buckling lengths can be used when the plate is loaded in tension: $L_1 = e_2$ for Leg 1, and $L_2 = e_1$ for Leg 2. For plates loaded in compression, the buckling length extends approximately to the center of the adjacent leg. For design purposes, the following buckling lengths can be used when the plate is loaded in compression: $L_1 = e_2 + d_2/2$ for Leg 1, and $L_2 = e_1 + d_1/2$ for Leg 2.

1.3 Experimental Results

The nominal strength of each specimen was calculated using the proposed design method, and the results are summarized in the 2nd column of Table 1. All of the loads are expressed as the nominal brace load based on the minimum strength of the two legs. The predicted failure modes, based on the proposed design procedure, are listed in the 3rd column. The specimen numbers are suffixed with "T" if the plate was loaded in tension, and "C" if it was loaded in compression.

Spec. No.	P_n (kN)	Pred. Failure Mode	P_{ep} (kN)	P_{eu} (kN)	Exp. Failure Mode	$\frac{P_{ep}}{P_n}$	$\frac{P_{eu}}{P_n}$
2T	221	I	307	400	I	1.39	1.81
6T	201	E	188	238	I	0.938	1.19
8T	307	I	379	406	I	1.24	1.32
9T	239	I	229	283	I	0.960	1.19
10T	368	I	428	489	I	1.16	1.33
1C	176	I	148	204	I	0.843	1.16
2C	219	I	210	284	I	0.960	1.30
3C	187	I	207	286	I	1.11	1.53
4C	75.3	E	142	142	E	1.89	1.89
5C	104	E	128	208	I	1.23	2.01
6C	69.8	E	113	113	E	1.61	1.61
7C	235	I	206	207	I	0.877	0.880
8C	217	I	171	270	I	0.786	1.24
9C	166	I	197	229	I	1.19	1.38
10C	253	I	254	296	I	1.00	1.17

P_n = nominal strength (kN)
 P_{ep} = experimental load at proportional limit using 0.794 mm offset (kN)
 P_{eu} = maximum experimental load (kN)
 E Elastic lateral-torsional buckling
 I Inelastic lateral-torsional buckling

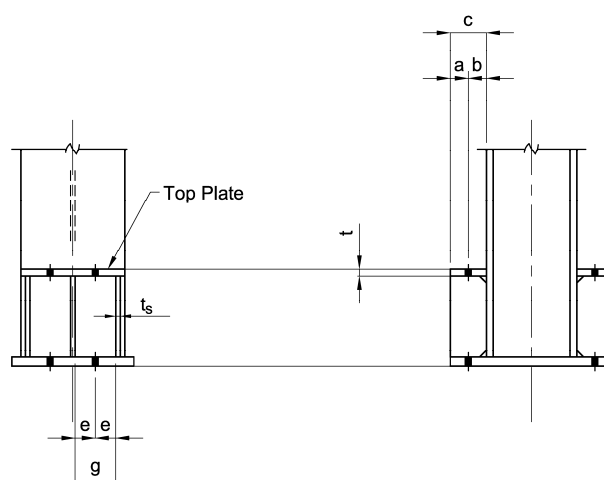
The experimental loads are listed in columns 4 and 5 of Table 1. P_{ep} is the experimental load at the proportional limit, determined using a line offset 0.794 mm from the linear portion of the experimental curve. P_{eu} is the maximum experimental load. The experimental failure modes are listed in column 6. The P_{ep}/P_n and P_{eu}/P_n ratios are listed in the 7th and 8th columns of Table 1, respectively. P_{ep}/P_n varied from 0.786 to 1.89 with an average of 1.15 and a standard deviation of 0.302. P_{eu}/P_n varied from 0.880 to 2.01 with an average of 1.40 and a standard deviation of 0.312.

2 BENDING OF TOP PLATES IN BASE CHAIR CONNECTIONS

In many heavy industrial facilities, column bases must transfer large uplift loads to the foundation. If the tension load is too large to carry with a standard base plate, chairs can be used to transfer the load. A base plate connection with a chair welded to each flange is shown in Figure 4.



a. base chair for heavy industrial facility



b. base chair arrangement and dimensions

Figure 4. Column base plate connection with chair.

Base chairs are also used at the bottom of plate and shell structures such as tanks, silos and stacks, as shown in Figure 5. For these structures, the top plate can be a continuous ring or separate plates at each anchor rod.

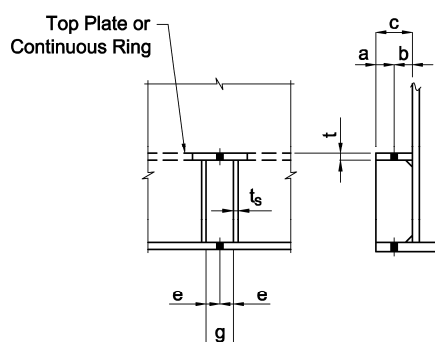


Figure 5. Base chair configuration for plate and shell structures.

The top plate thickness has traditionally been determined using the elastic one-way bending capacity of a beam spanning the distance between the vertical stiffener plates (AISI, 1992; Bednar, 1986; Mahajan, 1975), or the two-way bending capacity based on elasticity theory

(Troitsky, 1982). These design methods can be used where the nominal stress must be limited to the elastic range, such as structures subject to fatigue. However, for static loads, a more realistic design model can be achieved by considering the plastic capacity of the plate in two-way bending. In this paper, the yield line method will be used to derive an equation to determine the ultimate bending capacity of continuous and non-continuous top plates.

2.1 Yield Line Solution for Top Plate

Based on the yield line pattern in Figure 6, Dowswell (2010) derived Equation 7.

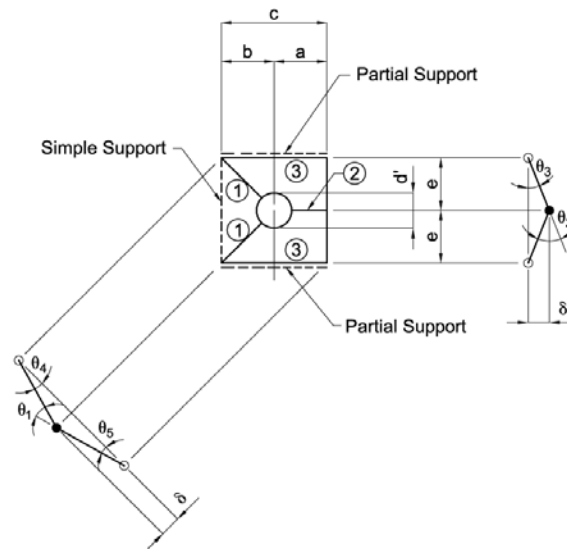


Figure 6. Yield line model for top plate bending.

$$T = \frac{F_y t^2}{2} \left[\frac{e}{b} + (1 + \alpha) \frac{c}{e} - \frac{d'}{2e} \right] \quad (7)$$

where

- F_y = specified minimum yield strength of the top plate, MPa
- T = tension in the anchor rod, N
- a = distance from the center of the hole to the edge of the top plate, mm
- b = distance from the center of the hole to the face of the support, mm
- c = $a + b$
- d' = hole diameter, mm
- e = distance from the center of the hole to the inside edge of the vertical stiffener plate, mm
- t = thickness of the top plate, mm
- α = reduction factor to account for the effect of partial fixity of the outer yield lines (discussed in detail in the next section)

2.2 Partial Fixity at Outer Yield Lines

Equation 7 contains a factor, α , to account for the effect of partial fixity of the outer yield lines (yield lines 3), where $0 \leq \alpha \leq 1$. For top plates that are continuous over the stiffeners, the outer yield lines can be assumed fully fixed. For discontinuous top plates, the design can be based on the conservative assumption that the outer yield lines are simply supported. For these cases, the values for α are

- $\alpha = 1$ for continuous top plates fixed against rotation at both outer yield lines
- $\alpha = 0$ for top plates that are free to rotate at both outer yield lines

If flexural continuity is provided between the top plate and the vertical side plates, the bending strength of the vertical plates can be used to provide partial fixity to the outer yield lines on the top plate. In the presence of axial loading, Neal (1961) showed that the plastic capacity of a member with rectangular cross section is reduced according to Equation 8, which gives the reduced moment capacity per inch of the vertical side plate.

$$m'_{ps} = m_{ps} \left[1 - \left(\frac{P}{P_y} \right)^2 \right] \quad (8)$$

where

m_{ps} = full plastic moment capacity per inch of the vertical side plate, N-mm/mm
 $= F_{ys} t_s^2 / 4$

P = compression load in the vertical side plate, N

P_y = yield load of the vertical side plate, N
 $= F_{ys} b_s t_s$

F_{ys} = specified minimum yield strength of the vertical side plates, MPa

b_s = width of the vertical side plates, mm

t_s = thickness of the vertical side plates, mm

If the vertical side plate has the same width as the top plate, the fixity factor for the outer yield lines can be calculated using Equation 9.

$$\alpha = \frac{F_{ys}}{F_y} \left(\frac{t_s}{t} \right)^2 \left[1 - \left(\frac{P}{P_y} \right)^2 \right] \quad (9)$$

2.3 Proposed Design Method

It is proposed that Equation 7 be used for design of top plates in base chair connections. To account for the upper bound nature of the solution and the corner effect, Wood (1961) recommended an additional design margin of 15% for yield line solutions. Kennedy and Goodchild (2003) recommended an additional margin of 10%. Based on these values, it is recommended that $\phi = 0.80$ be used as the reduction factor for limit states design methods.

3. FATIGUE OF COPED BEAMS

When beams are connected to girders at the same elevation, the beam must be coped to allow proper erection clearance as shown in Figure 7. Coped beams with cyclic loads are common in bridges and industrial structures supporting vibrating machinery. When these beams are subjected to repeated loading cycles, the reentrant corner of the coped web can develop fatigue cracks. Fisher (1984) has documented several cases of fatigue cracking at coped beams.

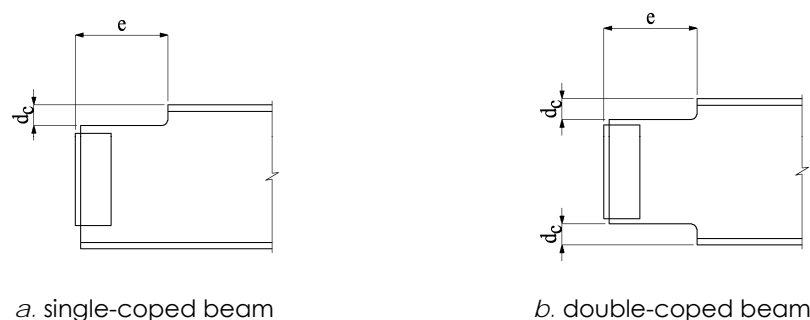


Figure 7. Coped beams.

Because the beam end connections are normally idealized in design as frictionless pins, the top edge of the cope is in flexural compression and the bottom is in tension as shown in Figure 8. Therefore, it is clear that, for double-coped beams, the bottom cope is a potential location for fatigue cracking. Although fatigue is usually considered only when at least part of the load cycle causes tensile stresses, experimental evidence and in-service cracks have shown that beam copes subjected to nominally compressive stresses can develop fatigue cracks. This is due to at least two factors: 1. flexural tension stresses along the coped edge due to partial fixity of the end connection; 2. tensile residual stress caused by the cutting operation.

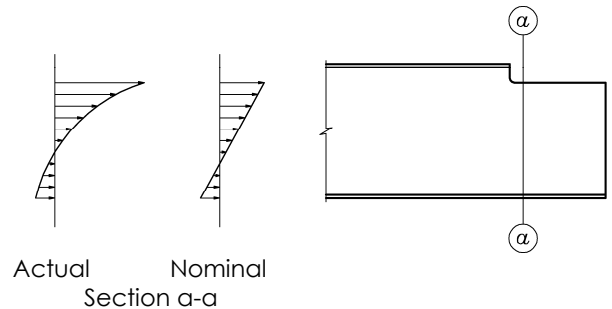


Figure 8: Bending stress at beam cope.

Copes are commonly manufactured by flame cutting which can reduce the fatigue life of the cut edge by introducing tensile residual stresses and causing metallurgical changes, which lead to hardened, brittle material in the heat affected zone. Stress concentrations at the reentrant corner, as shown in Figure 8, will further reduce the fatigue life. On a smaller scale, stress concentrations due to the roughness of the cut edge (Poor Workmanship) can reduce the fatigue life as well.

A literature review revealed adequate resources, including 41 tests from three independent research projects, to establish a design procedure based on the existing literature. Therefore, the existing research was reviewed to determine the factors influencing fatigue life and to formulate a design proposal.

3.1 AISC Specification

AISC Specification (AISC, 2010) Appendix 3 classifies coped beams as a Category B detail. The design stress range is

$$F_{SR} = \left(\frac{329C_f}{n_{SR}} \right)^{0.333} \geq F_{TH} \quad (10)$$

where

- F_{SR} = design stress range, MPa
- C_f = constant from Table A-3.1
= 120×10^8 for Category B
- n_{SR} = number of stress range fluctuations in design life
- F_{TH} = threshold allowable stress range, MPa
= 110 MPa for Category B

According to AISC Specification (AISC, 2010) Appendix 3, Section 3.5, "Reentrant corners at cuts, copes and weld access holes shall form a radius of not less than 3/8 in. (10 mm) by predrilling or subpunching and reaming a hole, or by thermal cutting to form the radius of the cut. If the radius portion is formed by thermal cutting, the cut surface shall be ground to a bright metal surface." Additionally, Section 3.5 requires that "The surface roughness of flame

cut edges subject to significant cyclic tensile stress ranges shall not exceed 1,000 $\mu\text{in.}$ (25 μm), where ASME B46.1 is the reference standard."

3.3 Existing Research

Several research projects have been conducted that are relevant to the fatigue of coped beams. Of particular interest are the full-scale tests on coped beams and beams with web openings. Supporting information was found on the effect of fabrication methods and quality of fabrication, and the effect of cope geometry on the stress concentration factor.

Yam and Cheng (1990) studied the fatigue life of coped steel beams. They tested nine full-scale specimens with varying stress ranges and cope radii. The specimens were fabricated from W410x54 rolled shapes of CSA G40.21-M81 300W material. The cope length was 230 mm and the cope depth was 60 mm. The radii of the reentrant corner varied from 10 mm to 30 mm. To study the effect of different fabrication methods, the copes were formed with three different methods. They tested six flame-cut specimens without further preparation and two specimens that were flame cut and ground smooth. They also tested one specimen that started the cope by drilling a hole at the cope corner, and finished by flame cutting.

From the strain gage readings and finite element data, it was determined that a highly localized stress concentration exists at the edge of the cope. A stress concentration factor, C , which is defined as the ratio of the maximum longitudinal stress at the reentrant corner to the elastic stress calculated using simple bending theory, was determined in the study. Equation 11 was developed by curve fitting the finite element data.

$$\log(C) = 0.937 - 0.285 \log(r) \quad (11)$$

where

r = cope radius, mm

Roeder et al. (2005) tested 16 coped beams to determine the effectiveness of several damage limitation methods. The beams were W21x62 of A572 Grade 50 steel with constant or variable amplitude loading. For the variable amplitude tests, Miner's rule was used to determine the effective stress range. Specimens 0A and 0B had square-cut copes, and the remaining specimens were fabricated to a 22 mm radius. Most of the specimens had a rating of 250ST, which is a very high quality flame-cut edge. To determine the effect of poor workmanship, eight of the specimens were intentionally fabricated with notches between 1.6 and 3 mm. The authors concluded that relatively smooth flame-cut copes (250ST or better) can be designed using Fatigue Category D and rough or notched copes crack at levels well below Category E'.

Frost and Leffler (1971) tested five W16x36 and four W14x38 beams in fatigue with rectangular web holes. The beams were fabricated with ASTM A36 steel. The hole depth to beam depth ratio was approximately 0.5, and the corner radii varied from 3.3 mm to 48 mm. Two hole length to hole depth ratios were used: 1.2 and 1.5. The fabrication methods included machine cutting, flame cutting, and flame cutting with grinding.

Theoretical and experimental stress concentrations at the reentrant corners were between 1.2 and 2.9. The researchers concluded that the fatigue life depends on the stress concentrations at the reentrant corner, which are highly dependent on the corner radii. They suggested a minimum corner radius of 25.4 mm and noted that the fatigue life correlated reasonably well with the fatigue results on plain material if the stress concentrations are accounted for.

Table 2 summarizes the specimens and results from the three research projects. The experimental fatigue life, N, in column 6 is the number of cycles to initial crack formation at the reentrant corner. Some of the tests were stopped before the specimen formed a crack; therefore, these were excluded from the data pool.

Table 2. Description of specimens and experimental results.					
Specimen	Reentrant Corner Radius r (mm)	Fabrication Method	Surface Roughness R_a (μm)	Nominal Stress Range F_{SR} (MPa)	Fatigue Life N (Cycles)
Yam and Cheng (1990)					
CB-0	0	F	NR	50.6	162,500
CB-10A	15.0	F	NR	50.6	405,800
CB-20B	25.0	FG	NR	50.6	8,632,000
CB-20A	25.0	F	NR	50.6	1,080,000
CB-30	32.0	F	NR	50.6	1,390,000
CB-10B	15.0	F	NR	40.5	928,000
CB-10C	15.0	F	NR	71.2	292,500
CB-10D	15.0	FG	NR	71.2	318,600
CB-10E	10.0	D	NR	71.2	211,500
Roeder et al. (2005)					
0A	0	F	6.35	48.2	385,000
0B	0	F	6.35	48.1	980,000
1	22.0	F	6.35	90.8	1,675,000
2	22.0	F	6.35	110	450,000
3	22.0	F	6.35	76.1	3,672,500
3B	22.0	F	6.35	88.0	2,050,000
4B	22.0	F	6.35-12.7	78.2	3,102,100
5	22.0	FN	3.18	79.6	1,550,000
6	22.0	FN	6.35-12.7	75.4	75,000
7	22.0	FN	3.18	102	25,000
8	22.0	FN	6.35	97.8	5,000
9	22.0	FN	6.35-12.7	115	50,000
10	22.0	FN	6.35	90.8	150,000
11	22.0	FN	6.35	31.8	50,000
12	22.0	FN	≥ 12.7	84.5	200,000
Frost and Leffler (1971)					
1A	3.30	FG	1.27	142	65,700
2A	3.30	FG	1.27	192	48,000
3A	3.30	FG	1.27	158	200,000
4A	3.30	FG	1.27	115	543,000
5A	3.30	FG	1.27	119	621,200
7A	16.0	M	0.813	147	757,000
8B-2	7.87	F	10.2	153	163,000
8B-3	7.87	F	10.2	125	986,000
9B-2	16.0	F	11.2	146	562,000
F Flame-cut FG Flame-cut with edges ground smooth FN Flame-cut with notches D Drilled, then flame-cut M Machined NR Not Reported					

3.4 Results

The results in Table 2 are plotted in Figure 9 for the nominal stress range, along with the fatigue curves for Stress Categories A through E'. The specimens are divided into three categories for plotting: 1. Specimens with $r \geq 9.53$ mm (hollow circle), 2. Specimens with $r \geq 25.4$ mm (solid circle), 3. Specimens that are not classified (\times). The specimens that are not classified were either fabricated with $r < 9.53$ mm or were intentionally fabricated with a notch at the cut edge. Several of the specimens with $r < 25.4$ mm plotted below the curve for Stress Category E'.

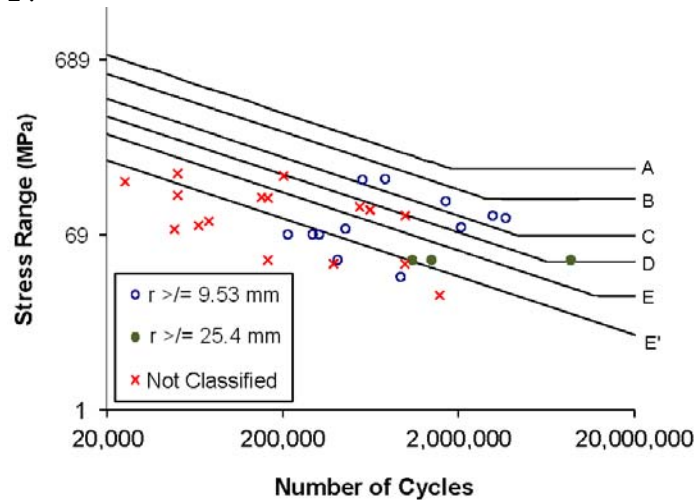


Figure 9: Fatigue data using nominal stress range.

As expected, the fatigue life increased with increasing radius. This is because the specimens with a larger cope radius had a smaller stress concentration. Figure 10 was plotted with a stress range, F'_{SR} , which is the maximum longitudinal stress at the reentrant corner, calculated with Equation 12.

$$F'_{SR} = CF_{SR} \quad (12)$$

The fatigue life of the specimens correlated reasonably well with Stress Category B. Specimens with $r = 0$ and specimens that were intentionally fabricated with a notch at the cut edge were assigned a stress concentration factor of 6. Specimens with $0 < r < 9.53$ mm were assigned a stress concentration factor of 4. These values appear to provide a good correlation with the experimental results with the exception of Roeder et al. (2005) Specimen 11, which falls well below Stress Category B.

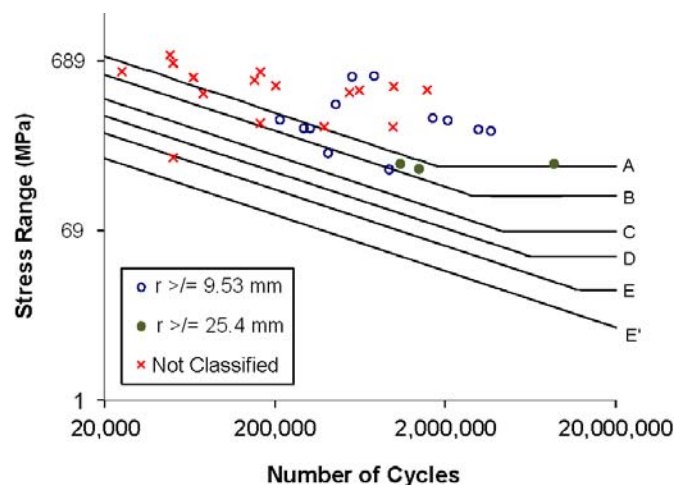


Figure 10: Fatigue data using stress concentration factor.

3.5 Design Recommendations

It is proposed that the design stress range be determined with Equation 10 for Stress Category B. This should be greater than the required stress range calculated with the stress concentration factor according to Equations 11 and 12. Alternatively, if $r \geq 25.4$ mm, coped beams can be designed using Stress Category E' with the stress range defined using the nominal stress.

REFERENCES

1. AISC (2010), Specification for Structural Steel Buildings, June 22, American Institute of Steel Construction, Chicago, IL.
2. AISI (1992), Steel Tanks for Liquid Storage, Steel Plate Engineering Data—Volume 1, American Iron and Steel Institute, Washington, DC.
3. ASME (1996), Surface Texture (Surface Roughness, Waviness, and Lay), ASME B46.1-1995, The American Society of Mechanical Engineers, June 14.
4. Bednar, H.H. (1986), Pressure Vessel Design Handbook, 2nd Ed., Krieger Publishing Company, Malabar, FL.
5. Dowswell, B. (2010), "Bending of Top Plates in Base Chair Connections," Engineering Journal, American Institute of Steel Construction. Fourth Quarter, Vol. 47, No. 4.
6. Dowswell, B. (2005), "Design of Wrap-Around Steel Gusset Plates," Ph.D. Dissertation, Department of Civil and Environmental Engineering, The University of Alabama at Birmingham.
7. Dowswell, B. (2004), "Lateral-Torsional Buckling of Wide Flange Cantilever Beams," AISC Engineering Journal, Third Quarter, pp. 135-147.
8. Fisher, J.W. (1984), Fatigue and Fracture in Steel Bridges: Case Studies, John Wiley and Sons, New York, pp. 302-310.
9. Frost, R.W. and Leffler, R.E. (1971), "Fatigue Tests of Beams with Rectangular Web Holes," Journal of the Structural Division, American Society of Civil Engineers, Vol. 97, No. ST2, February.
10. Kennedy, G. and Goodchild, C. (2003), Practical Yield Line Design, British Cement Association, Crowthorne, England.
11. Mahajan, K.K. (1975), "Tall Stack Design Simplified," Hydrocarbon Processing, September, pp. 217-220.
12. Neal, B. G. (1961), "The Effect of Shear and Normal Forces on the Fully Plastic Moment of a Beam of Rectangular Cross Section," Journal of Applied Mechanics, Vol. 28, pp. 269-274.
13. Roeder, C.W., MacRae, G., Leland, A., and Rospo, A. (2005), "Extending the Fatigue Life of Riveted Coped Stringer Connections," Journal of Bridge Engineering, ASCE, Vol. 10, No. 1, January/February, pp. 69-76.
14. Troitsky, M.S. (1982), Tubular Steel Structures—Theory and Design, The James F. Lincoln Arc Welding Foundation, Cleveland, OH.
15. Wood, R.H. (1961), Plastic and Elastic Design of Slabs and Plates, Ronald Press, New York.
16. Yam, M.C.H. and Cheng, J.J.R. (1990), "Fatigue Strength of Coped Steel Beams," Journal of Structural Engineering, ASCE, Vol. 116, No. 9, September, pp. 2447-2463.